

A comprehensive study of the 2019-2020 flare of OJ 287 in X-ray window using *Swift*, *XMM-Newton*, *NuSTAR*, and *AstroSat*

Raj Prince,^{1*} Gayathri Raman,^{2,3} Rukaiya Khatoon,⁴ Aditi Agarwal,⁵ Varun,⁶ Nayantara Gupta,⁵ Bożena Czerny,¹ and Pratik Majumdar,⁷

¹Center for Theoretical Physics, Polish Academy of Sciences, Al.Lotnikow 32/46, Warsaw, Poland

²Indian Institute of Technology Bombay, Powai, Mumbai-400076, India

³Department of Astronomy and Astrophysics, The Pennsylvania State University, 525 Davey Lab, University Park, PA 16802, USA

⁴Tezpur University, Napaam-784028, Assam, India

⁵Raman Research Institute, Sadashivanagar, Bangalore 560080, India

⁶Aryabhata Research Institute of Observational Sciences (ARIES), Manora Peak, Nainital 263002, India

⁷Saha Institute of Nuclear Physics, HBNI, Kolkata, West Bengal, 700064, India

Accepted XXX. Received YYY; in original form ZZZ

ABSTRACT

OJ 287 is a well studied binary black hole system, that occasionally exhibits bright X-ray and optical flares. Here we present a detailed spectral study of its second brightest X-ray flare observed during 2019-2020. Various X-ray instruments were used to capture this historic moment. Their data is analysed and modeled along with optical and UV data. Based on *Swift*-XRT and UVOT observations, the entire period is divided in three states, defined as low, middle, and high state. The results of our analysis suggest a “softer-when-brighter” behavior. We proposed a Target of Opportunity (ToO) observation using *AstroSat* to compliment this study along with the *Swift*-XRT, *XMM-Newton*, and *NuSTAR* observations. Simultaneous X-ray spectra observed by various instruments during high states is very steep and agree with each other within the errorbar. A significant spectral change is observed in optical-UV and X-ray spectrum during the high flux state, suggesting the emergence of a new HBL component. A significant shift of two orders of magnitude in the synchrotron peak is observed as the source evolves from low flux to high flux state. The emergence of new HBL component could be associated with the increase in accretion rate post BH-disk impact and eventually it could trigger the flare produced in jet. Color-magnitude diagram reveals a “bluer-when-brighter” chromatism during the flaring period. Different chromatism or no chromatism at various occasions suggests a complex origin of optical emission, which is believed to be produced by disc impact or through synchrotron emission in the jet.

Key words: galaxies: active – galaxies: jets – galaxies: nuclei – quasars: individual (OJ 287) – X-rays: galaxies

1 INTRODUCTION

Blazar OJ 287, having the most massive black hole among all blazars, is located at a redshift 0.306 (Mao 2011). It is classified as BL Lac object in the 3FGL (Acero et al. 2015) & 4FGL (Abdollahi et al. 2020) catalog. It is known for its high radio, optical, X-ray, and γ -ray variability. The variability time scale ranges from hours to decades across the wavebands (Goyal 2018). OJ 287 got more attention after the detection of high optical activity recurring at a regular interval of 12 years periodicity. In fact, this was the first AGN classified as a blazar, whose periodic behaviour was observed after

analysing its century long optical light curve, which challenges the general scenario of blazars where flares or high activity states are randomly produced or in other words blazars have very stochastic variability across the electromagnetic spectrum. Periodic behavior observed in optical light curve encouraged many authors to study this source in detail and provide the possible physical explanation of periodic behavior that is new to a blazar. In literature, Sillanpaa et al. (1988) proposed a model of binary black hole system where they associated the periodic variations to tidally induced mass inflows from accretion disk into the black hole (BH). They suggested that during the periastron passage, i.e., when the secondary black hole passes close to the primary BH, an optical outburst is produced. It has been observed that sometimes

* E-mail: raj@cft.edu.pl

flares appear a bit earlier or a bit later than their predicted time, which is difficult to explain from first principles for a binary BH model. Later, [Lehto & Valtonen \(1996\)](#), have performed a detailed analysis of substructure inside the major flares and they modified the Binary BH model to explain the sharp flare. In their model the secondary BH crosses the accretion disk of primary BH and produces the major optical flares. Other possible models have also been proposed in the recent past. The study of [Britzen et al. \(2018\)](#) considering the 15 GHz radio observation suggests the highly Doppler-boosted jet emission for major flare and the precession of jet to explain the periodicity in the light curve. Their model suggests that the optical emission is produced due to synchrotron radiation of relativistic electrons inside the jet. Many more studies suggest that the BBH model is more successful in explaining the double-peaked optical flare ([Dey et al. 2018](#)). In the Binary BH model it is shown that the impact of the secondary onto the accretion disk of the primary BH creates two hot bubbles of gas on both sides of the disk which radiate in optical through thermal Bremsstrahlung after becoming optically transparent. Since the secondary BH crosses the disk two times in each orbit, a double-peaked flare is observed/produced. The orbital period of the secondary BH is associated with the ~ 12 years periodicity seen in the light curve. Recent study by [Dey et al. \(2018\)](#) has confirmed the presence of 24 flares between 1888 to 2015 by the BBH model. The 2015 flare was also explained by [Dey et al. \(2018\)](#) in the context of binary black hole model. [Valtonen et al. \(2019\)](#) have estimated the values of the physical parameters of the impact of secondary onto the accretion disk of the primary BH in the BBH model.

In the past decade many broadband studies have been carried out on this source. In the broadband analysis, this source is classified as a low-peaked BL Lac source where the synchrotron emission is constrained by NIR to soft X-ray as the synchrotron peak in the spectral energy distribution (SED) lies below 10^{14} Hz. The high energy hump of the SED generally covers the X-ray and gamma-ray frequencies, with the peak at around 0.1 GeV to few GeV ([Abdo et al. 2010](#), [Kushwaha et al. 2013](#)). Synchrotron self-Compton (SSC) is the most well accepted mechanism that can explain the second SED peak. However, in some flares it has been found that the SSC model is not sufficient to explain the high energy part of the spectrum and hence people have used additional external thermal field to explain this. In [Kushwaha et al. \(2013\)](#), they have used external photon field at a temperature of 250 K as a source of external seed photons. These photons get up-scattered by the highly relativistic electrons present in the jet through the inverse-Compton mechanism.

In X-rays, this source has been studied in detail during several active states. The maximum number of observations with the longest durations have been carried out with the *Swift* -XRT telescope, which nicely covered many bright X-ray flares of OJ 287. From the earlier X-ray flares it has been found that OJ 287 sometimes shows a significant change in the optical-UV and X-ray spectrum and that eventually leads to the shift in synchrotron peak towards higher energy during flare. Significant change in the X-ray spectrum and emergence of new HBL component is very rare in blazars. However, this kind of behavior has been seen in a few sources studied in the past ([Pian et al. 1998](#), [Raiteri et al. 2015](#), [Kapanadze et al. 2018](#), [Kushwaha et al. 2018a,b, 2020](#)).

In 2020, a bright optical-UV, and X-ray flare was reported in various ATels¹ ([Zola et al. 2020](#), [Komossa et al. 2020b](#), [Reinhart et al. 2020](#), [Hosokawa et al. 2020](#), [Komossa & Grupe 2020](#)). Recently, [Komossa et al. \(2020a\)](#) presented a detailed analysis with the data from *XMM-Newton* and *NuSTAR* telescopes. Many *XMM-Newton* archival observations along with recent 2018 and 2020 observations were analysed and they found that the spectrum in 2020 behaves very differently from archival observations including the year 2018. They suggested a non-thermal origin of the 2020 flares. We have performed a broadband SED modeling of the flares during 2017–2020 and it is presented in Prince et al (under-review).

In this work, we provide a detailed analysis of *Swift*-XRT and UVOT instrument data and report the emergence of a new HBL component which eventually leads to the shift in synchrotron peak towards higher energy. The synchrotron emission is constrained by the optical-UV and X-ray data. Emergence of HBL component in low BL Lac blazars is very rare. We also carried out a Target-of-Opportunity (ToO) observation of the source using India's first space-based multi-wavelength mission, *AstroSat* ([Agrawal 2017](#)). The results from Soft X-ray focusing Telescope (SXT) and Large Area X-ray Proportional Counter (LAXPC) instrument of *AstroSat* are also discussed in this work. At the end we have discussed the color-magnitude diagram followed by the summary and conclusions.

2 X-RAY ANALYSIS

Swift-XRT:

On February 3, 2017, an X-ray flare was observed by the *Swift* telescope ([Gehrels et al. 2004](#)), and the results was reported in Atel 10043 ([Grupe et al. 2017](#)). It is reported as the brightest flare ever detected since the monitoring of the *Swift* telescope. After that, many multiple flares were observed in X-rays between 2019 and 2020, and this period has been studied in this paper. *Swift* is a space-based telescope with three instruments on-board, observing all kinds of Galactic and extra-galactic sources in soft & hard X-rays, Optical, and UV simultaneously. The working energy range of *Swift*-XRT is 0.3–10.0 keV. The BL Lac OJ 287 was observed by *Swift*-XRT telescope during the multiple flaring episodes in X-ray frequencies between the period November 2019 to May 2020. We have analyzed all the observations done during this period. The raw data processing was carried out using the task '*xrtpipeline*²' and cleaned events file were produced for each observation. The CALDB version 20160609 was used while processing the raw data. Our analysis is focused on only the Photon Counting (PC) mode observations and the *Xselect* tool is used for source and background selection. We have selected a region of 12 arc seconds around the source and away from the source for the source and background, respectively, in our data analysis. The *Xselect* tool was further used to extract the spectrum and light curve, and the modeling of the spectrum has been carried out using *XSPEC* ([Arnaud 1996](#)). For modeling the spectra, we have used

¹ <http://www.astronomerstelegam.org/?read=13677>

² <https://heasarc.gsfc.nasa.gov/ftools/caldb/help/xrtpipeline.html>

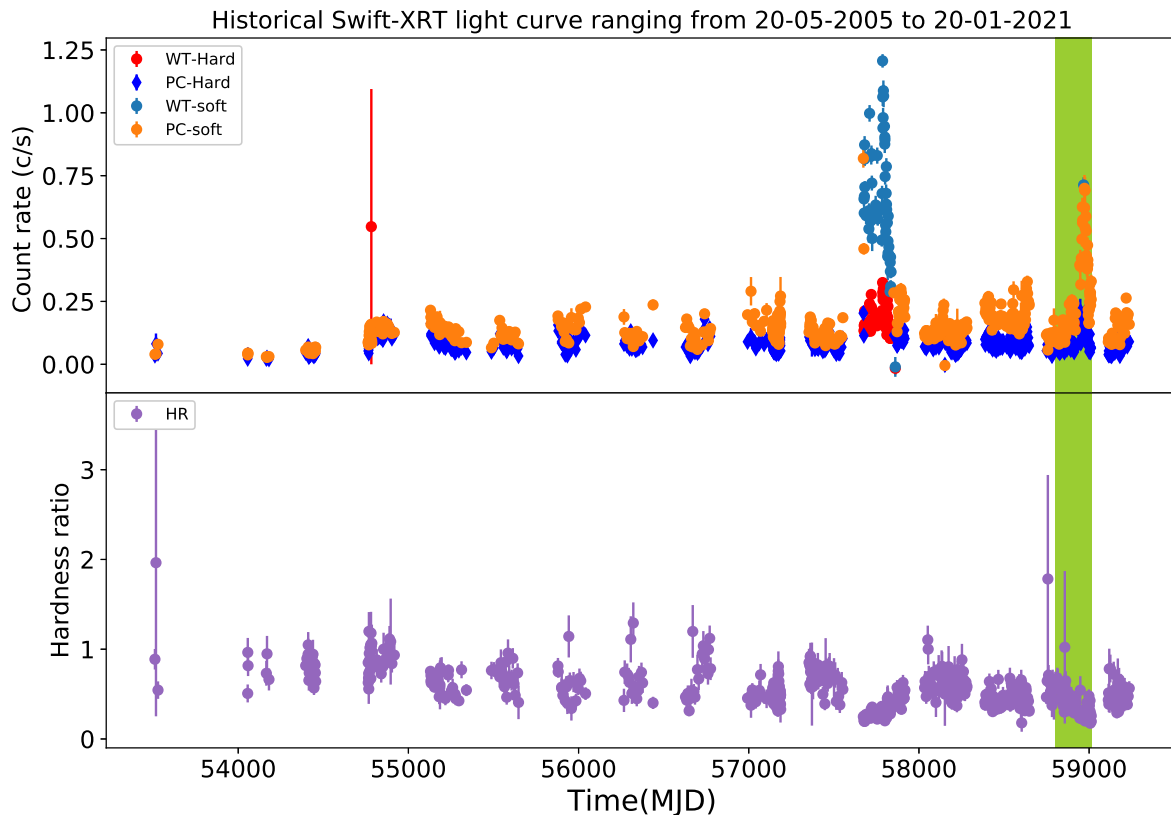


Figure 1. Long-term X-ray light curve from *Swift* -XRT. WT: Window timing, PC: Photon Counting, Hard: 1.5-10.0keV, Soft: 0.3-1.5 keV.

a absorbed power-law/log-parabola model. During fitting, the Galactic absorption column density $n_H = 3.04 \times 10^{20} \text{ cm}^{-2}$ is fixed from [Dickey & Lockman \(1990\)](#). The modeling is done for an energy range of 0.3–10.0 keV.

AstroSat-SXT: The SXT observations were carried out in the Photon Counting (PC) mode and the Level-1 data was further reduced using the `sxtpipeline1.4b` (Release Date: 2019-01-04) to generate the Level-2 data products ([Singh et al. 2016, 2017](#)). The events from the various orbits were merged using the `SXTEVTMERGERTOOL` in Julia. Further, we used the merged event list for temporal and spectral analysis. The merged event files were accessed by the tools `Xselect` where a source region of 10 arcsec was chosen around the source and the blank sky for the background. The response files and the background spectra are provided by the SXT-POC (Payload Operation Center) team. Finally, the grouped spectra were fitted in `Xspec` in the 0.3–10 keV band, and χ^2 statistic was obtained for the best fit.

AstroSat-LAXPC: LAXPC ([Yadav et al. 2016](#)) is designed to observe sources in a very wide range of X-rays ranging from 3 keV to 80 keV. It has three identical proportional counters (LAXPC10, LAXPC20, & LAXPC30) onboard the *AstroSat* satellite. Data used in this work is taken from the LXP20 detector. The LAXPC30 detector is switched off due to gain instability issues. The data reduction and further pro-

cessing of Level-1 were carried out using the LAXPC data analysis pipeline version 3.1³. The pipeline code combines data from multiple orbits and also filters out overlapping segments between each orbit. Using the standard pipeline `laxpc_make_event`, we generate the cleaned event file. A good time interval (GTI) window was applied during the processing using the `laxpc_make_stdgti` tool, in order to exclude the time intervals corresponding to the Earth occultation periods, SAA passage and standard elevation angle screening criteria. Since Blazars are observed as a faint sources in LAXPC, we adopted the faint source pipeline for the spectral analysis. In order to reduce background contribution from all LAXPC layers, only the top detector layer was used for the timing and spectral analysis of the LXP20 data.

XMM-Newton: Blazar OJ 287 was observed with XMM-Newton ([Jansen et al. 2001](#)) with an exposure time of 15 ks between 2020-04-24 21:13:18 to 2020-04-25 01:23:18 UTC. The data is publicly available on the HEASARC webpage and denoted as OBS-ID 0854591201. *XMM-Newton* data was reduced with Science Analysis Software (SAS) version 18.0.0. First, we created the EPIC-PN event list using `epproc` com-

³ Data analysis software was obtained from <http://astrosat-ssc.iucaa.in/?q=laxpcData>

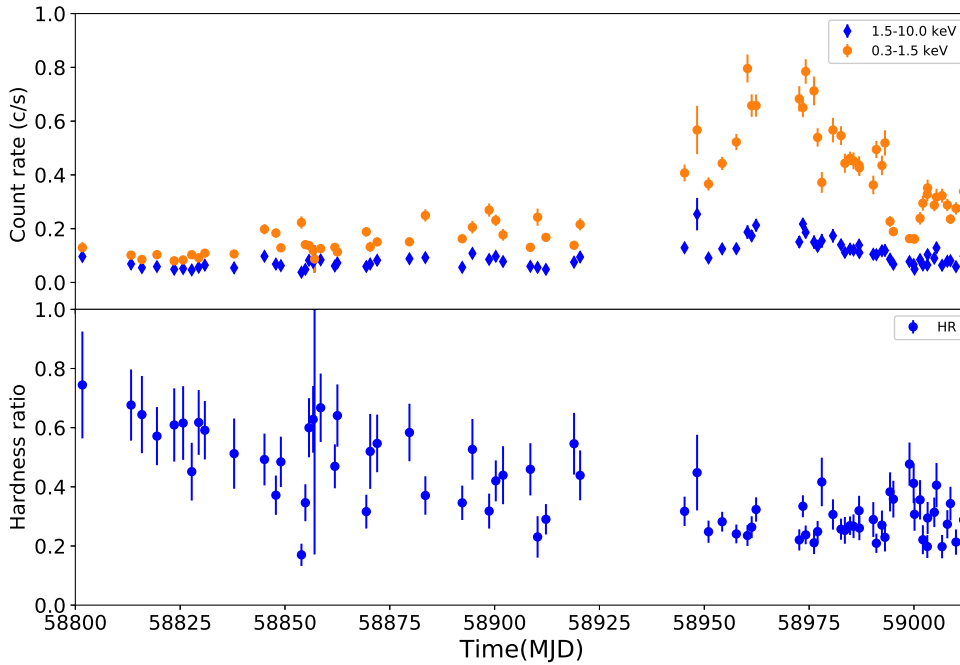


Figure 2. This shows the light curve in hard and soft state. Lower panel shows the hardness ratio.

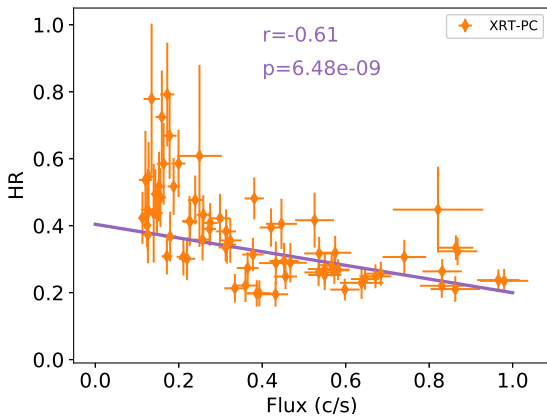


Figure 3. Hardness ratio plotted against the total (0.2-10.0 keV) flux.

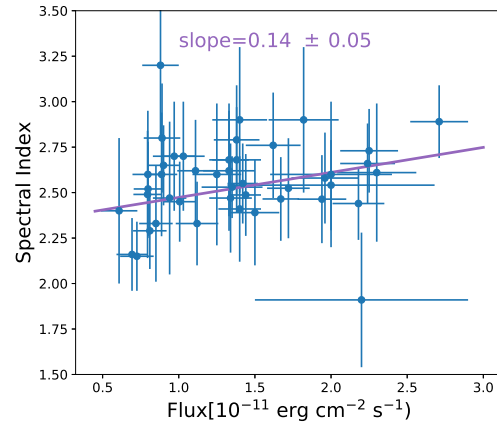


Figure 4. The spectral index plotted against the high state flux, suggesting a “softer-when-brighter” trend.

mand in SAS. Then, we examined the the single event high energy light curve to identify the intervals of flaring particle background and filter the event list for those time intervals. EPIC-PN light curve and spectra were extracted from a circular region of $50''$ centered on the source position, and background were collected from a nearby region of same size. We also examined the pileup very carefully using `eptaplot` and found no significant pileup during this observation. Finally, we generated the RMF and ARF files using `rmfgen` and `arfgen` tools and grouped the data to have minimum of 20 counts in a bin.

NuSTAR: A ToO observation in *NuS-*

TAR (Harrison et al. 2013) was also performed during the high X-ray flux state on 2020-05-04 starting at 20:36:09 UTC with an effective exposure time of 29.5 ks. The data reduction is made using the latest *NuSTAR* data analysis software (NuSTARDAS) version 1.9.2 provided by HEASOFT. To extract the source spectrum and the background spectrum, a circular region of $20''$ and $50''$ were chosen around the source and away from the source, respectively.

3 OPTICAL AND UV OBSERVATIONS

Having the *Swift* Ultraviolet/Optical Telescope (UVOT, Roming et al. 2005) on board with *Swift*-XRT has the advantage of getting simultaneous observations in Optical and UV bands. *Swift*-UVOT has also observed the OJ 287 in all of the available six filters U, V, B, W1, M2, and W2, simultaneously with the X-ray observations. The source instrumental magnitudes are extracted following the `uvotsource` procedure. We have considered the region of 5 arcsec around the source as the source region, and the region away from the source as the background region. The magnitudes are corrected for galactic extinction by using the reddening $E(B-V) = 0.0241$ from Schlafly & Finkbeiner (2011) and zero points from Breeveld et al. (2011). Moreover, the magnitudes are converted into flux by multiplying by the conversion factor estimated by Poole et al. (2008) and the ratios of extinction to reddening from Giommi et al. (2006).

4 RESULTS

4.1 X-ray Light curves

XRT: We have produced the long term X-ray light curve of OJ 287, using *Swift*-XRT observations which is shown in Figure 1. The XRT observed the source in two different modes **Photon Counting (PC)** mode and **Window Timing (WT)** mode. In Figure 1, it is observed that the source showed a very bright soft-X-ray flare in 2016-2017, which was studied in detail earlier by Kushwaha et al. (2018b). In 2020, the second brightest soft-X-ray flare was observed as also marked by color patch in Figure 1. Our focus is to study the 2020 flare in detail and compare it with the older 2016-2017 flare.

Figure 2 shows the patched part of the light curve. The soft (0.3–1.5 keV) and hard (1.5–10.0 keV) light curves are shown in two colors, and the lower panel shows the hardness ratio, which is defined as the ratio of hard count to soft count. From the upper panel it is clear that the Blazar OJ 287 is highly variable and flaring in soft X-rays, while the count rate is lower and the source is far less variable in the hard X-ray band. In the beginning of the light curve (at MJD 58800), the fluxes are almost similar in both the bands, but as time passes, the soft X-ray part starts rising slowly with respect to hard X-ray. During April 2020 (~MJD 58940), the soft X-ray flux is almost four times higher than the hard X-ray flux. It remained in a very high state for an entire month till May 2020 because of which the flare was eventually recognized as the second brightest X-ray flare in the history of OJ 287. To characterize the variability in the soft and hard X-ray band, we have estimated the fractional variability (F_{var}) amplitude (Vaughan et al. 2003). The source is found to be more variable in 0.3–1.5 keV band with $F_{\text{var}} = 0.38 \pm 0.01$ and less variable in 1.5–10 keV band with $F_{\text{var}} = 0.27 \pm 0.01$. In the lower panel it can be seen that, as the source flux increases, the hardness ratio starts to shift towards the lower value. To see the clear trend in the hardness ratio (HR), we have plotted the hardness ratio against the total (0.3–10.0 keV) flux in Figure 3. The HR is anti-correlated with the total flux with Pearson’s correlation coefficient 0.61, suggesting a “softer-when-brighter” trend. We have also plotted the power-law spectral index against the X-ray (0.3–10.0 keV) flux in Figure 4. We have observed a clear “softer-when-brighter” trend fitted with

a straight line with slope 0.11 ± 0.05 . For the highest flux, the spectral index is as soft as ~ 2.8 as seen in Figure 4. The “softer-when-brighter” trend in X-ray is a prevalent behavior in history of OJ 287 except the flare in 2015 where the spectrum was rather harder with flux. Comparing the softer behavior detected in the current flaring state, with the harder behavior observed in the 2015 flare, we conclude that both the flares may have a different origin.

SXT: We carried out a Target of Opportunity observation using *AstroSat* (ObsID: 9000003672) during the X-ray flare in May 2020, since an enhanced X-ray flux was reported in several ATels. The source was observed from 15th–19th May, 2020. We have analyzed all the observations separately. In some of the observations, *AstroSat* detected a very low count rate and was heavily background dominated. Due to poor statistical quality of the data from those Obs IDs, we did not carry out any timing or spectral study for those observations. The SXT spectral products corresponding to May 15, 2020 had a good signal to noise ratio (SNR) for meaningful spectral study, which we have discussed in Section 4.4.

LAXPC: Along with SXT, simultaneous LAXPC observations were carried out between May 15, 2020 to May 19, 2020. (ObsID: 9000003672). We carried out a similar data reduction process for all the observational data taken during this period. As was the case with SXT, only the data of the observation corresponding to May 15 had a good SNR and is therefore presented in this paper. All the other observations were of poor statistical quality and background dominated and we do not utilize them for this study. The simultaneous observations by LAXPC with SXT provide an opportunity to model both the spectra together. The result of this joint fit is discussed in section 4.4.

XMM-Newton: We checked for recent archival *XMM-Newton* observations of OJ 287. We obtained a 15 ks long observation dated April 24, 2020, whose data data was publicly available on the HEASARC webpage⁴. Recently, Komossa et al. (2020a, 2021) have used this observation for the spectral study, where they have compared the 2020 spectrum with the older spectrum from this source, and they noticed a significant change in the shape of the spectrum. We have produced the *XMM-Newton* lightcurve which does not show significant variability of the source, therefore we did not use it in our study. Further, we extracted the spectrum using XMM observation and discussed about it in the later section 4.4.

Nustar: We also looked for the timing analysis in *Nustar*, but were unable to extract any light curve. Therefore, the study is focused on understanding the spectral behavior. Detailed discussion is provided in Section 4.4.

4.2 Optical-UV and γ -ray Light Curves

In Figure 5, we have shown the simultaneous gamma-ray, X-ray, optical and UV light curves during the flaring period of the source from MJD 58800 to 59012. It can be seen that the optical-UV emissions follow the X-ray emission, where they show an increase in brightness over time. Based on the average values of magnitudes (shown by a solid green line) observed in the optical-UV band, we divided the light curves

⁴ <https://heasarc.gsfc.nasa.gov/cgi-bin/W3Browse/w3browse.pl>

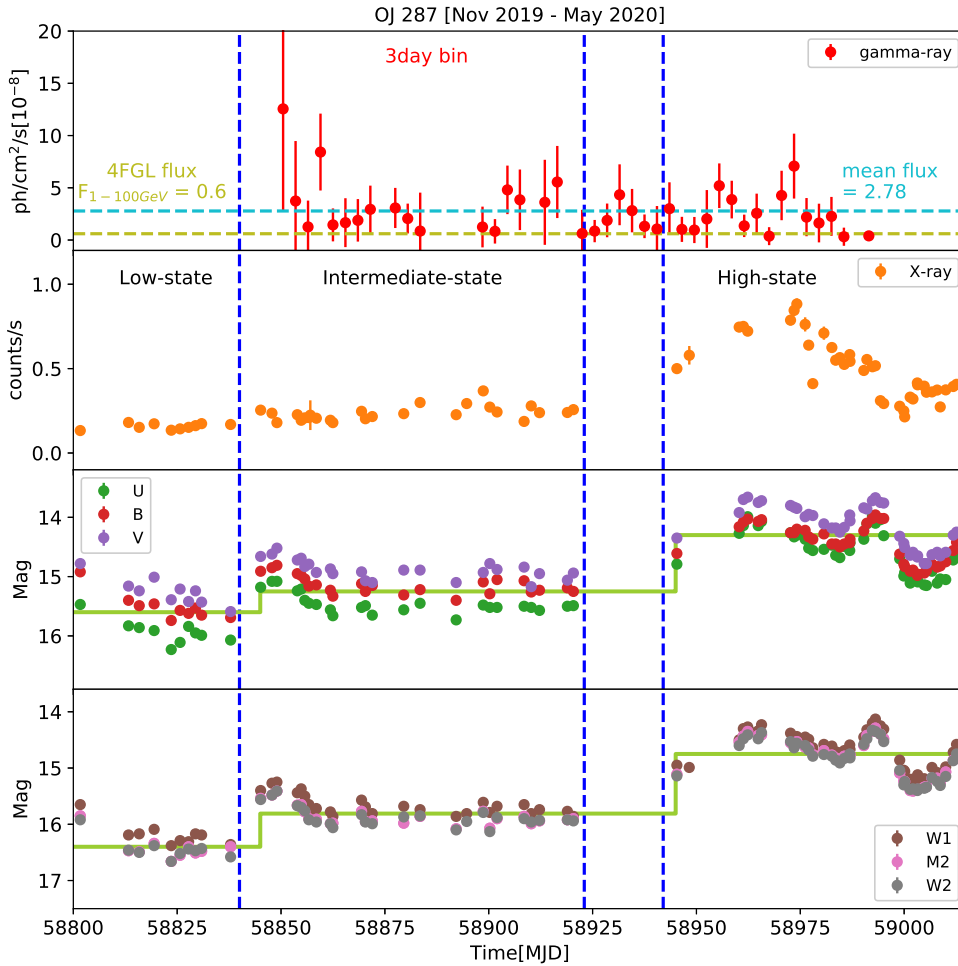


Figure 5. Broadband light curve created for period starting from November 2019 to current flaring state May 2020. Step plot in optical-UV is shown to identify the step-wise increase in their flux.

into three different parts, namely, low state, intermediate state, and high state. The solid green lines which represent the average values of the magnitudes in three different states are jointly represents a step function structure. In X-ray, the flux follows a similar kind of step function, but no apparent trend is seen. These three different states are used for the further study. No evident activity is seen in the γ -ray light curve shown in the uppermost panel. The flux observed in γ -rays is very low and mostly constant over time (fluctuating around the mean). The average flux during the flaring period is obtained as $2.78 \times 10^{-8} \text{ ph cm}^{-2} \text{ s}^{-1}$ and shown by a horizontal dashed line. Similarly, the 4FGL catalog flux is also represented by the horizontal dashed line in Figure 5 which is way below the average flux of the source during this period. Previous studies on the flares detected in 2015 and 2016-2017 by [Kushwaha et al. 2018a,b](#) also show no strong activity in γ -ray, though the source was flaring in optical-UV and X-rays.

4.3 X-ray Spectral Analysis

We have produced the X-ray spectrum of all the three states identified in Figure 5. The spectra are fitted with the simple power-law and the log parabola models, in built in `Xspec`, and a galactic absorption `tbabs` is added to the model. The final model we used is `tbabs*powerlaw/logparabola` and the best fit model parameters are presented in Table 1. We have also carried out an `F-test` to determine the best model for the X-ray spectral fitting. It is considered that, if the the null hypothesis probability (p-value) is below 0.01 the log parabola model is preferred over the power-law model. In our study, we always found that the p-value > 0.01 which suggests the power-law is preferred over log parabola model. To estimate the flux and error bar on flux, we have used an additional component to the model in `XSPEC`, called `cflux`. It is noted that the power-law spectral index changes from low state to high state.

The power-law spectral index can be seen changing from

low state to high state. During the low state, the power-law flux is estimated as $(5.15 \pm 0.15) \times 10^{-12}$ erg cm $^{-2}$ s $^{-1}$ with the photon spectral index (Γ), 1.89 ± 0.07 and the reduced $\chi^2 \sim 0.99$. In the intermediate state, the flux is $(7.14 \pm 0.08) \times 10^{-12}$ erg cm $^{-2}$ s $^{-1}$ and the Γ is 2.15 ± 0.04 and the fit has the reduced $\chi^2 \sim 1.15$. Similarly, during the high state the averaged flux is $(14.72 \pm 0.09) \times 10^{-12}$ erg cm $^{-2}$ s $^{-1}$ with $\Gamma = 2.56 \pm 0.02$, and the reduced $\chi^2 \sim 0.91$. It shows a clear trend of “softer-when-brighter” behavior of the source OJ 287, during a long time-scale. The spectrum produced for all the three states is shown in Figure 6, which clearly show that the shape of the spectrum is also changing when the source transitions from the low state to the intermediate state and finally to the high state.

We have also extracted the spectrum from the optical-UV band, and similar to the case in X-ray spectrum, a significant change is noticed here as the source transitions from the low state to the high flux state. The combined optical-UV and X-ray spectrum for all the three states is shown in Figure 7, suggesting a significant change in the combined spectrum, which leads to an emergence of a new HBL component. The change in optical-UV and X-ray spectrum suggests a shift in the synchrotron peak of the broadband SED towards higher energy. As a result, OJ 287, a well-known LBL (Nilsson et al. 2018) blazar, behaves like an HBL type source. A recent study of the kinetic features of radio jet blazars classifies OJ 287 as IBL type blazar (Hervet et al. 2016). The details about the new HBL component are discussed in section 5.

All X-ray spectrum and the corresponding UVOT spectrum are shown in Figure 7. The shape of the spectrum is flipping around a pivotal energy value corresponding to $\sim 10^{18}$ Hz as the source changes its states. In the UVOT spectrum, it is found that the spectrum is quite steep during the low state, and then it becomes flat in the intermediate state, and finally, in the high state, it is increasing with energy. The change in the UVOT and the X-ray spectrum together can be helpful to determine the peak of the synchrotron emission. In the next section, we have modeled the UVOT and X-ray spectrum for a better understanding of the synchrotron peak during various states.

4.4 *Swift*-XRT, *XMM-Newton*, *NuSTAR*, and *AstroSat* Spectral Analysis

In this section, we present the spectral analysis of simultaneous and quasi-simultaneous X-ray, and UV-optical observations shown in Figure 8. We have one *XMM-Newton* observation on April 24, 2020 (MJD 58963.88), one observation of *NuSTAR* on May 04, 2020 (MJD 58973.86), and one observation of *AstroSat*-SXT on May 15, 2020 (MJD 58984.0). We also looked for simultaneous observations with *Swift*-XRT and found several XRT observations that were mostly simultaneous with the other missions. Since *XMM-Newton* and the *AstroSat*-SXT have the same operating energy range (0.3–10.0 keV) as the *Swift*-XRT, we have compared their simultaneous spectrum in Table 2. In Figure 8 corresponding to *XMM-Newton* observation, we have three close *Swift*-XRT observations, and the combined spectrum (individual observation has similar spectrum) of these three XRT observations is compared with the *XMM-Newton* spectrum by plotting them together in Figure 9. The XRT spectrum is fitted with power-law (PL) and log-parabola (LP) models separately.

However, comparing these models with the F-test statistics suggests that the PL model fits the spectrum better than the LP model. The *XMM-Newton* spectrum gives a better fit with PL+LP combination. Finally, the model used to fit the XRT spectrum is `tbabs*powerlaw` or `tbabs*logparabola` and for the XMM spectrum it is `tbabs*(powerlaw+logparabola)`. The best fit parameters are following, in case of XRT spectral fitting the powerlaw spectral index, Γ is obtained as 2.57 ± 0.09 with $\chi^2(\text{dof})=91.34(99)$, and the LP spectral index α is 2.57 ± 0.10 , curvature parameter $\beta = 0.21 \pm 0.33$, and $\chi^2(\text{dof})=92.40(100)$. In *XMM-Newton* spectrum, the spectral index for PL is $\Gamma = 2.27 \pm 0.42$ and the spectral index for LP is $\alpha = 3.45 \pm 0.32$ and the curvature parameter is $\beta = 0.73 \pm 0.36$ with the χ^2 value of 128.38(126) from the combined (PL+LP) modeling. These results suggest that, the LP spectrum using *XMM-Newton* observation is much steeper compared to the PL and LP spectrum observed from XRT. Alternatively, the XRT spectrum is steeper using the PL and LP models, than the *XMM-Newton* spectrum with PL model.

In the case of the simultaneous *NuSTAR* and *Swift*-XRT observations, we have fitted the joint *Swift*-XRT and *NuSTAR* spectrum to have a clear understanding of the broadband spectrum. The *Swift*-XRT observation with ObsID:35905053 is simultaneous to the *NuSTAR* observation, and hence a joint XRT+*NuSTAR* fit is produced, and a joint spectral fit of XRT+*NuSTAR* observations is shown in Figure 10. The joint fitting is performed in *Xspec* with a power-law spectral model. It is found that a single power-law can explain the total spectrum ranging from 0.3–50.0 keV. The model used for fitting is `constant*tbabs*powerlaw`. The component `constant` is added to match the normalization of both the data group and `tbabs` is used to account for galactic absorption. The best fit power-law index is found to be 2.37 ± 0.09 and the flux estimated in 0.3–10.0 keV is $(2.10 \pm 0.07) \times 10^{-11}$ erg cm $^{-2}$ s $^{-1}$ and the flux in 3.0–50.0 keV is found to be $(6.34 \pm 0.20) \times 10^{-12}$ erg cm $^{-2}$ s $^{-1}$.

AstroSat SXT and LAXPC observations are simultaneous as marked in Figure 8. The joint SXT+LAXPC spectral fitting is done using the power-law model along with the galactic absorption and the constant factor, same as described in the above section. The spectral fitting plot is shown in Figure 11. The spectral model `constant*tbabs*powerlaw` is used to model the spectrum. The simultaneous XRT observation corresponding to ObsID 00035905063 was also analyzed separately, and the spectral index was found to be 2.67 ± 0.14 . Comparing this value with the $\Gamma = 2.43 \pm 0.09$ obtained from the joint SXT+LAXPC spectral fit, suggests that the XRT spectrum is comparatively steeper than the joint SXT+LAXPC spectrum. The shape of the joint spectra of XRT+*NuSTAR* and SXT+LAXPC are consistent with each other.

The best fit parameters of all the simultaneous and quasi-simultaneous spectra are presented in Table 2.

5 MODELING THE SYNCHROTRON PEAK: HBL LIKE COMPONENT

This section is dedicated to identifying the change in the synchrotron peak as the source travels from low state to high flux state. Generally, the synchrotron peak in blazars can be constrained by the near-infrared and optical-UV emission along

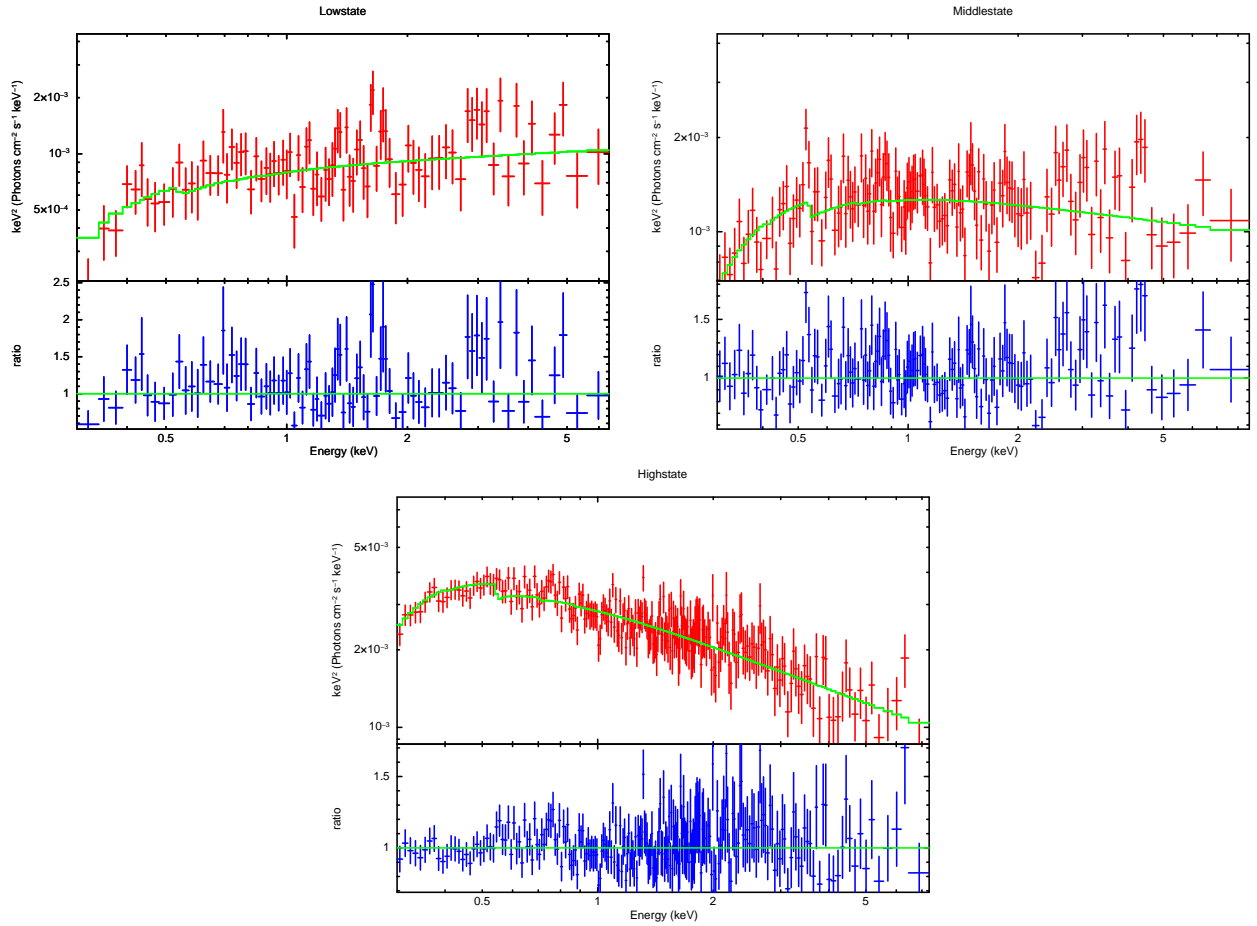


Figure 6. X-ray spectrum for all the three states fitted by powerlaw.

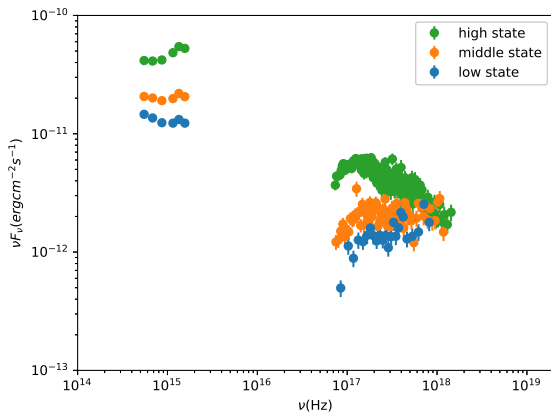


Figure 7. Combined broadband spectrum of all states. A clear spectral change is observed from low state to higher state.

with the soft X-ray emission. Here we have used optical-UV and X-ray spectrum to identify any changes in the location of the synchrotron peak during two different flux states. The general approach that is typically adopted in order to determine the location of the synchrotron peak is based on the log-parabolic modeling of NIR, optical-UV, and X-ray spectrum (Massaro et al. 2004, Kapanadze et al. 2018). Raiteri et al.

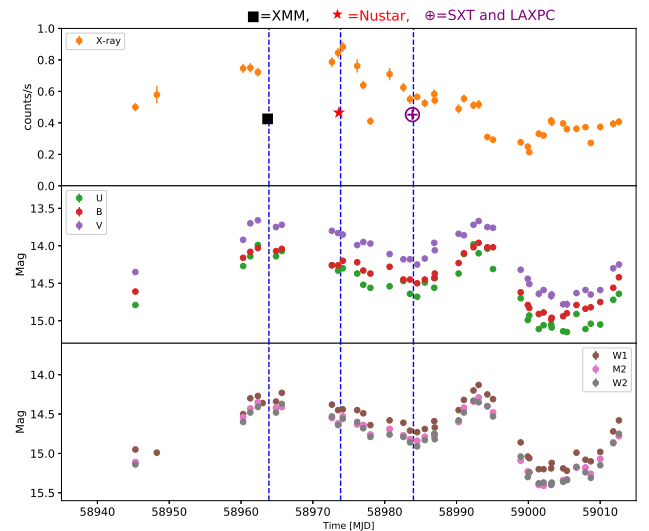


Figure 8. Broadband light curve of 2020 along with the simultaneous observations in other X-ray low and high energy band.

(2013) have used the log-cubic model to fit the spectrum from NIR to X-ray in order to constrain the exact location of the synchrotron peak in LBL BL Lac blazar. Here, we have used

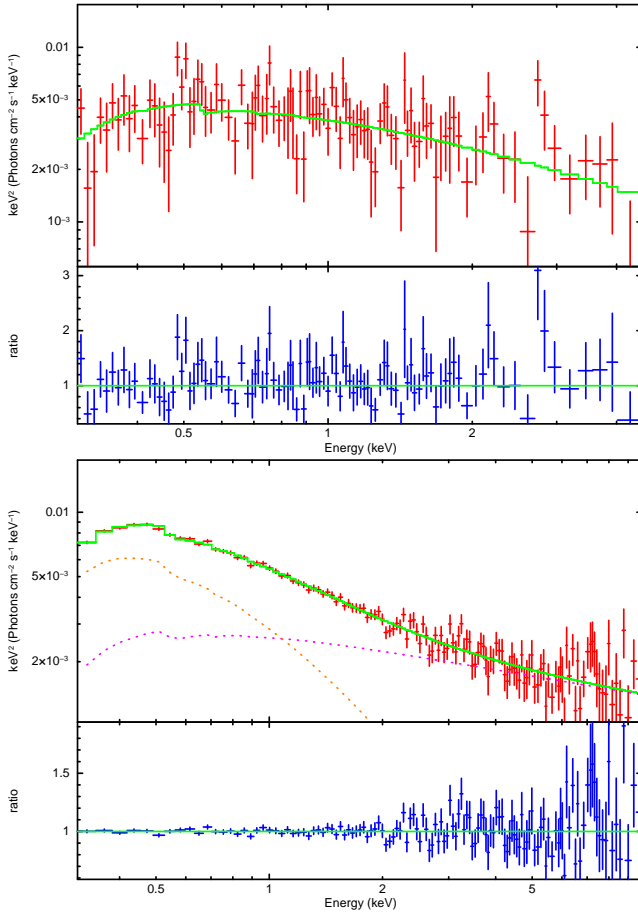


Figure 9. The two spectra are almost simultaneously observed in XRT and *XMM-Newton*. We have compared their spectra to see if they show the same behavior in *Swift*-XRT and *XMM-Newton* or not, discussed in section 4.4 in detail. Upper panel shows XRT and lower panel shows the *XMM-Newton* spectrum.

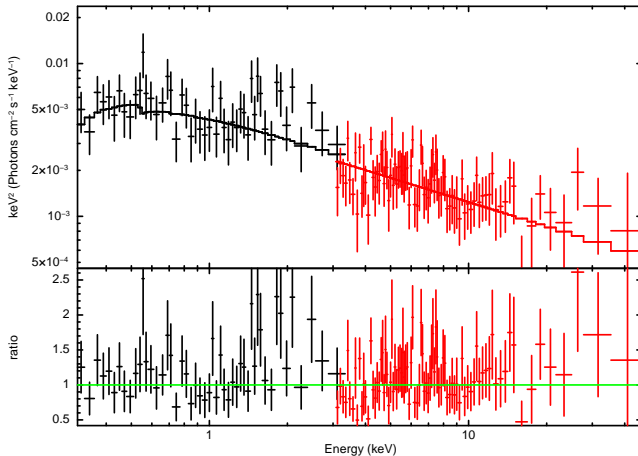


Figure 10. Joint XRT+*NuSTAR* fitting of the simultaneous observations. Black data points shows the *Swift*-XRT result and the red data points are the simultaneous *NuSTAR* results.

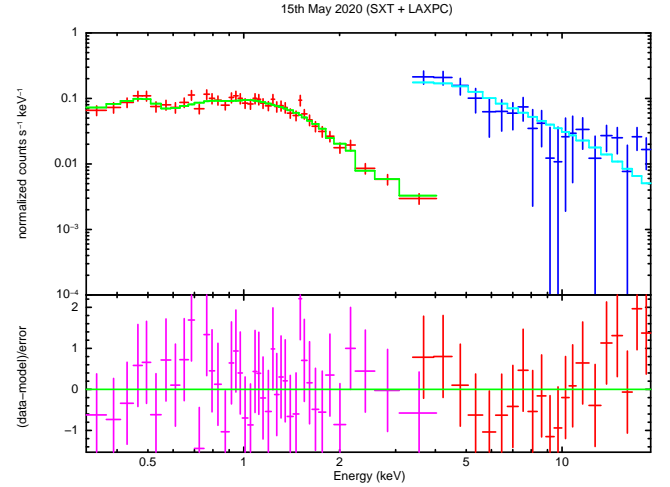


Figure 11. Joint *AstroSat* SXT+LAXPC fitting for the simultaneous observations done on May 15, 2020. In upper panel, red data points represent the SXT data and blue data points are the data from LAXPC.

a different approach, we have modeled the optical-UV and X-ray data points with the synchrotron process to estimate the precise location of the synchrotron peak.

The broadband spectral energy distribution of blazars exhibit a two hump structure located at low and high energy. The low energy hump covers the energy from infra-red to soft X-ray and high energy hump lies between hard X-ray to γ -ray. The low energy hump is well described by the synchrotron emission produced by the motion of relativistic charged particle in the jet magnetic field. To examine the position of synchrotron peak, we have modeled the optical-UV and X-ray emission together with the synchrotron model from publicly available code GAMERA, and modeling details can be found in Prince et al. (2021). We found that during the low state of the source, the synchrotron peak is observed at around $\sim 10^{14}$ Hz, which is the synchrotron peak assigned for the LBL type source (Padovani & Giommi 1995, Abdo et al. 2010). During the intermediate state, the X-ray spectrum does not change much, however a marginal shift of the synchrotron peak towards the higher energy is observed because of change observed in UVOT spectrum (Figure 12). During the high flux state, the shape of the UVOT and X-ray spectrum both have changed significantly compared to the low flux state, suggesting the emergence of a new HBL component in this source. The fitting of the parameters using GAMERA shows that a higher magnetic field (~ 6.7 G) is required in high flux state. However, in the low and intermediate state the magnetic field is found to be ~ 4.1 G. The LP electron distribution is provided to GAMERA to model the synchrotron peak. The spectral index, α is 1.8 for low and intermediate state and a steeper spectral index of 2.56 is required for the high state. Our modeling also suggests the need for higher energy electrons during high state compared to low and intermediate state. The values of the parameters obtained in this work are consistent with the parameters estimated in Prince et al. 2021 (under review). Modeling of the synchrotron emission shows that the synchrotron peak is shifted towards the higher energy, and the current peak location is around 10^{16} Hz, which is the ideal

case for the HBL type BL Lac source (Padovani & Giommi 1995, Abdo et al. 2010). The shift is two orders of magnitude in frequency which is very rarely seen in a single blazar. The results suggest that during the flaring period, the source exhibits very different spectral properties compared to when it is in a normal state. The result is shown in Figure 12. In OJ 287, this behavior was also seen before during the flare of 2016-2017 (Kushwaha et al. 2018b) where the synchrotron peak was shifted towards the higher energy. The first appearance of the HBL component was seen in a flare of 2017, the study of Kushwaha et al. (2020) discussed the disappearance of the HBL component in 2018. Again the HBL component appeared in the flare of 2020 as mentioned by Komossa et al. (2020a), Kushwaha et al. (2020), which has also been found in the present study. This finding suggests that the source is highly variable and changes its behavior during high flux state and fluctuates between LBL and HBL type source, and has an identity crisis. The blazar classification into FSRQ and BL Lac, and further the classification of BL Lac objects into LBL, IBL, and HBL is based on the fixed location of the synchrotron peak (Abdo et al. 2010). Therefore, the change in the synchrotron peak is not very common, and if it does occur, it challenges the understanding of the underlying physical mechanisms in these types of sources. Blazar OJ 287 is a well accepted binary black hole system, and the significant change in the optical-UV and X-ray spectral state could be associated with the disk-impact scenario. However, in the binary black hole model, the black hole-disk impact was expected in July-September 2019, and because of the sun’s constraint it could not be observed using *Swift* but was observed by the *Spitzer Space Telescope* (Laine et al. 2020). Considering the spectral change is associated with the disk-impact scenario, the appearance of new HBL components in April-May 2020 is still puzzling and needs more future study to draw any reliable conclusion. One of the possible explanation for the new HBL component could be the increase in the accretion rate post BH-disk impact and consequently it could trigger the flare produced in the jet after a few months. The time delay observed around nine months between the impact and the time of flare is not easy to understand, since various physical conditions could be responsible for that (disk/corona properties and geometry, magnetic field geometry, shock formation in the jet).

In our first paper, we have modeled the broadband SED of 2020 flare along with a low state, and we found that one emission zone is sufficient to explain the total SED (Prince et al. 2021, under review).

Recent study by Komossa et al. (2021) has discussed the long term X-ray spectral behavior of the source. They analysed the *XMM-Newton* and *Swift* data from 2005–2020, and found that the X-ray spectrum is highly variable. They also mentioned that the X-ray spectrum covers all the behaviors seen in blazars from significant flat to very steep.

6 COLOR-MAGNITUDE DIAGRAM

Simultaneous monitoring of OJ 287 in various optical (U, B, V) bands allow us to study the color variation of the source. The color-magnitude diagram helps in understanding the origin of different physical processes responsible for the flux variations in blazars. We fit the plots of colour in-

dices (CIs) vs. magnitude (M) with straight lines (i.e $CI = m * M + c$) using which we estimated the fit values of the slope, m , the Spearman correlation coefficient r along with the corresponding null hypothesis probability, p which are summarized in Table 3. A positive slope (when the p value is < 0.05) indicates significant positive correlation between CI and blazar magnitude, which in turn points towards a bluer when brighter (BWB) or redder when fainter trend (H.E.S.S. Collaboration et al. 2014) in the target, while a negative slope implies the opposite i.e. redder when brighter (RWB) trend (Agarwal et al. 2019).

We have plotted the four color-magnitude diagram defined among B-V vs. B, U-V vs. U, U-B vs. U, and U-B vs. V, which are shown in Figure 13. The estimated values of r and p for all the cases are mentioned in each plot. In three cases, we have seen a very strong correlation with a correlation coefficient of 0.69, 0.84, and 0.77, respectively, suggesting a “bluer-when-brighter” chromatism. In the case of B-V vs. B, we did not find any strong correlation, however, the slope suggests RWB chromatism but could not be confirmed. A recent study by Siejkowski & Wiercholska (2017) also did not find any correlation in B-V vs. V color-magnitude diagram. They have also not found any correlation in other combinations. However, our study shows a strong correlation and a strong BWB chromatism (Figure 13).

The previous study on the color-magnitude diagram reveals various types of variations, including BWB and RWB trends. The observations collected in B and V bands during 1973-1976 have been studied by Carini et al. (1992), and their result shows a hint of BWB chromatism. Further, observations made in flaring state from 1993 to 1997 in R and V bands show clear BWB chromatism as studied by Dai et al. (2011). A weak color-magnitude correlation in V and J bands was reported by Ikejiri et al. (2011) from the observation made between 2008 May to 2010 January. A recent study by Wiercholska et al. (2015) found a weak or no correlation in the color-magnitude diagram on the longer timescale for the observations made in B and R bands from the ATOM telescope during 2007-2012. However, they claimed the BWB chromatism at shorter isolated intervals in the long-term light curve. Color-magnitude diagram during the flare of 2015 studied by Jermak et al. (2016) shows a BWB chromatism which is expected in BL Lac type blazar. A recent study by Gupta et al. (2019) has collected the data from various telescopes worldwide from 2016 September to 2017 November in BVRI bands, and their study shows a BWB chromatism in V-R and R-I colors with respect to R band magnitude. However, their Pearson’s correlation coefficient is below 50%. In our study, the data collected for the period of roughly one year between 2019 to 2020 shows a strong correlation in the color-magnitude diagram for U-V and U-B colors (Figure 13). A clear BWB and RWB and occasional lack of correlation in the color-magnitude diagram of OJ 287 indicate a complex nature of the physical process responsible for the optical emission in this blazar.

Further, we have also estimated the average optical spectral index following the expression from Wiercholska et al. (2015), the average spectral index, $\langle \alpha_{BR} \rangle$ is derived as,

$$\langle \alpha_{BR} \rangle = \frac{0.4 \langle B - R \rangle}{\log(\nu_B / \nu_R)} \quad (1)$$

Where $\langle B - R \rangle$ is the average color from any two bands, and

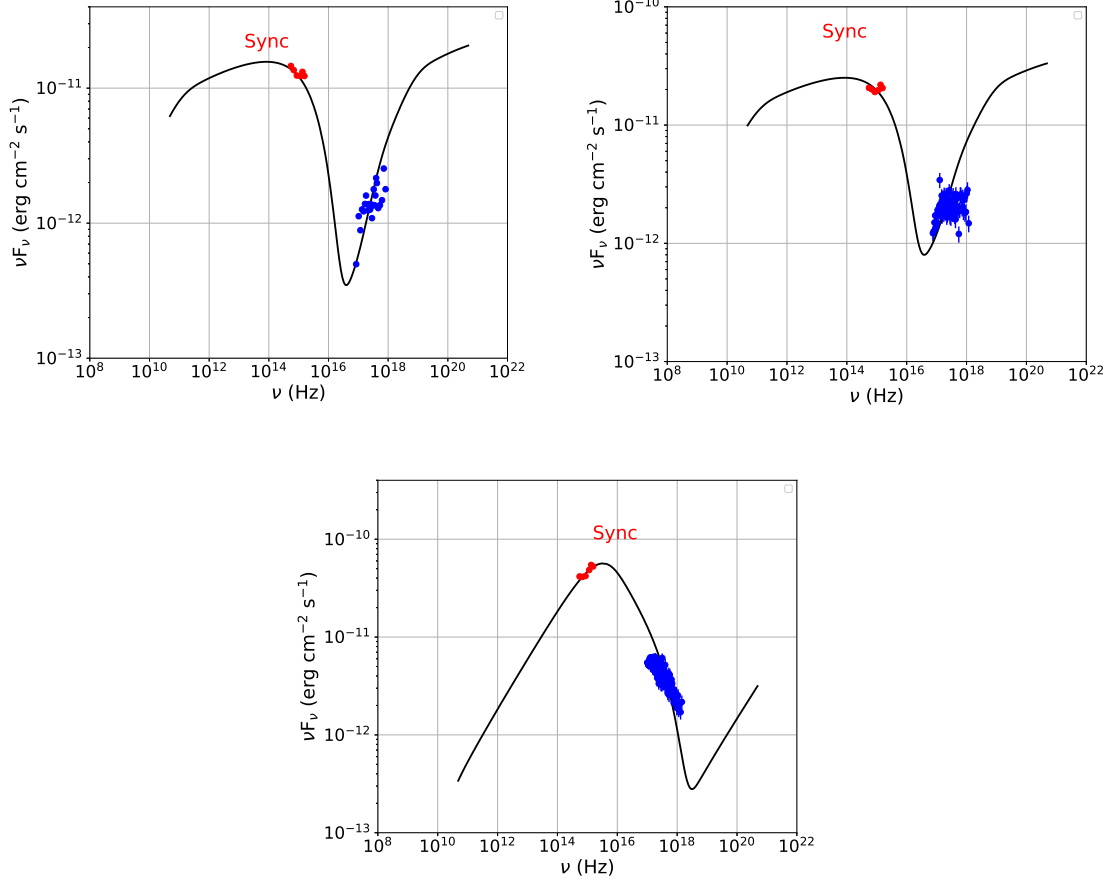


Figure 12. Broadband SED fit during the low, middle, and high state. The data points are from *Swift*-XRT/UVOT and the synchrotron peak is fitted with code GAMERA.

Observation ID	PL			LP			F-test	p-value	
	$F_{0.3-10keV}$	Γ	χ^2 (dof)	$F_{0.3-10keV}$	α	β			χ^2 (dof)
low state	5.15 ± 0.15	1.89 ± 0.07	85.30(86)	4.98 ± 0.20	1.86 ± 0.09	0.12 ± 0.21	84.46(85)	0.84	0.36
intermediate state	7.14 ± 0.08	2.15 ± 0.04	166.40(145)	7.22 ± 0.10	2.16 ± 0.05	0.04 ± 0.11	166.01(144)	0.34	0.56
high state	14.72 ± 0.09	2.56 ± 0.02	206.14(227)	14.60 ± 0.12	2.55 ± 0.02	0.04 ± 0.07	205.04(226)	1.21	0.27

Table 1. Modeled parameters for the X-ray spectrum during low state, intermediate state, as well as of high state. The fluxes are in unit of 10^{-12} erg cm^{-2} s^{-1} .

the ν_B , ν_R are the effective frequency of the corresponding B, and R bands. The optical spectral index estimated for the *Swift* U, B, V bands vary between 0.89 to 1.15, suggesting a significantly harder spectrum in optical bands. The optical spectral index is shown in Table 3. A significant spectral hardening in the optical emission is also seen in Kushwaha et al. (2020). During the same period, a significant spectral softening is observed in Figure 4, suggesting an anti-correlation with optical spectral index. Wierzcholska et al. (2015) have studied the large number of blazars and they found that the optical spectral index varies from extremely steep (>3) to

significantly flat (<0.5). In their study OJ 287 has a significantly steep optical spectrum, between, $\alpha_{BR} \sim 2-3$. In our study, the anti-correlation between optical and X-ray spectral index might suggests they are produced through different processes. Many more optical and X-ray study is required to come-up with any concrete conclusions.

Instruments and Dates	PL		χ^2 (dof)	LP			χ^2 (dof)	F-test	p-value
	$F_{0.3-10keV}$ ($F_{3.0-50.0keV}$)	Γ		$F_{0.3-10keV}$	α	β			
SXT + LAXPC	0.91 ± 0.04 (0.96_{-})	2.43 ± 0.09	40.25(57)	-	-	-	-	-	-
XMM (PL+LP) XRT	1.30 ± 0.90 1.93 ± 0.11	2.26 ± 0.42 2.57 ± 0.09	128.38(126) 91.34(99)	1.83 ± 0.16	3.45 ± 0.32 2.57 ± 0.10	0.73 ± 0.36 0.21 ± 0.34	- 92.40(100)	- 1.15	- 0.29
XRT + <i>NuSTAR</i>	2.10 ± 0.17 (0.63 ± 0.04)	2.37 ± 0.09	119.22(134)	-	-	-	-	-	-

Table 2. Modeled parameters for the simultaneous X-ray spectrum from XRT, SXT, XMM, *NuSTAR*, and LAXPC during various occasions. The fluxes are in unit of 10^{-11} erg cm^{-2} s^{-1} .

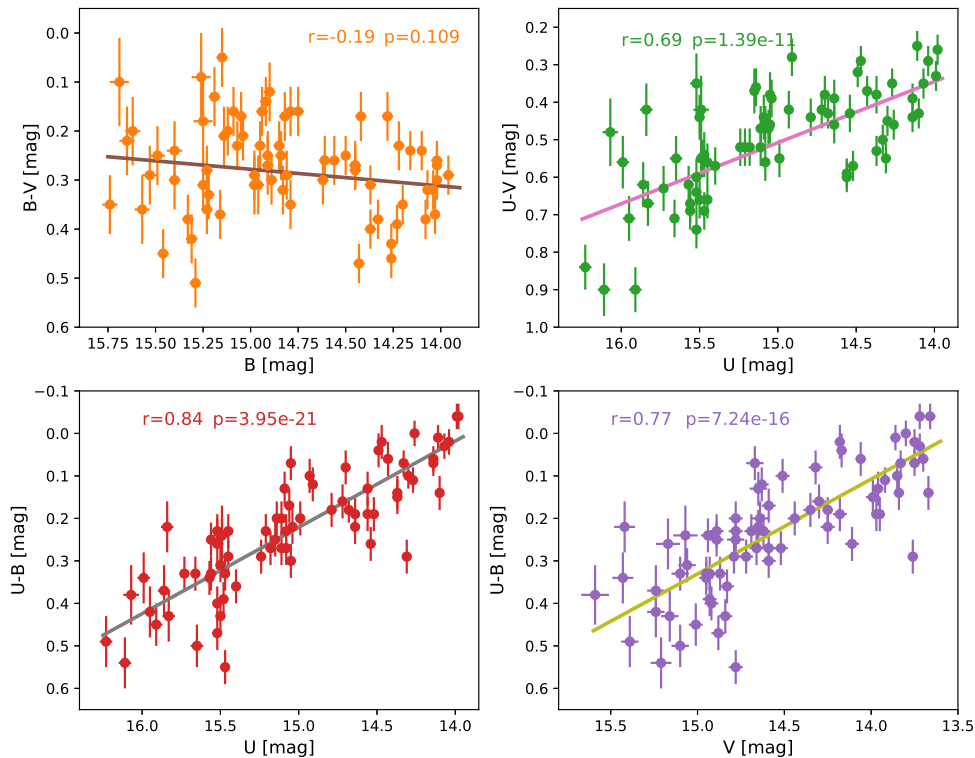


Figure 13. Colour-magnitude diagram during the 2020 flare.

7 SUMMARY AND CONCLUSIONS

Here we present a detailed X-ray and UV-optical study of the interesting blazar OJ 287 during its flaring activity between 2019 - 2020. The source was widely observed across the wavebands ranging from high energy γ -ray to down to the radio waveband. The source was found to be less variable in γ -ray, and it was reported to be flaring in various wavebands through various ATels. In *Swift*-XRT, the source was continuously monitored throughout the flaring period.

A 15 ks *XMM-Newton* observation was carried out during the peak of the X-ray flare and another ToO observation (~ 30 ks) was carried out using *NuSTAR*. These datasets are publicly available on the HEASARC webpage and are therefore used in this study. We proposed a ToO observation of OJ 287 in *AstroSat*, a broadband telescope operated by India, during the same period. The study includes the data from *AstroSat*-SXT and LAXPC instruments. The long-term *Swift*-XRT light curve shows that the 2020 flare is the sec-

Color	m	r	p-value	$\langle\alpha_{BR}\rangle$
B-V	-0.03	-0.19	0.109	1.15±0.22
U-V	0.16	0.69	1.39e-11	1.01±0.10
U-B	0.20	0.84	3.95e-21	0.89±0.17
U-B *	0.22	0.77	7.24e-16	-

Table 3. Color magnitude variations and their parameters. m = slope, r = Pearson’s correlation, p-value = Null hypothesis probability, U-B * = color variation with respect to V magnitude. The last column show the average optical spectral index.

ond brightest flare observed from this source. We produced the long-term light curve from November 2019 to May 2020, using *Swift*-XRT and UVOT observations, and divided them into three different states categorized as low state, intermediate state, and high state (Figure 5) based on the flux level in optical-UV bands. The flare of 2020 is categorized as a soft X-ray flare where the source is flaring in 0.3–1.5 keV band, while the flux is almost constant in the 1.5–10.0 keV band. A “softer-when-brighter” behavior is seen in the hardness ratio plot in Figure 3. The flux vs. index plot shown in Figure 4 also supports the “softer-when-brighter” behavior, mostly seen in BL Lac type of blazar. Joint spectral fitting of simultaneous observations of *Swift*-XRT and *NuSTAR*, and the *AstroSat*-SXT and LAXPC is presented in this work. In both cases the spectral model is fitted with power-law and the spectral index is found to be consistent with each other within the errorbar. The *Swift*-XRT spectral analysis along with the UVOT spectrum for the low, intermediate, and high state suggests a spectral evolution, and the result is shown in Figure 7. The spectral evolution suggests a shift in the synchrotron peak of the source towards the higher energy as shown in Figure 12. The shift in synchrotron peak suggests an emergence of HBL components during the high flux state. We have also studied the color-magnitude behavior of the source during this bright state, and results are shown in Figure 13. In B-V vs. B, we do not see any correlation. However, in other combinations, a significant correlation is observed between color and the magnitude of the source, suggesting a strong “bluer-when-brighter” chromatism. A significant harder spectrum is observed in optical which is anti-correlated with the X-ray emission. A significant spectral change between the current flaring state and the older flare in OJ 287 studied by many authors clearly suggests a complex behavior of the source. Much more detailed optical and X-ray study would be required to better understand this proposed binary black hole system.

ACKNOWLEDGEMENTS

The project was partially supported by the Polish Funding Agency National Science Centre, project 2017/26/A/ST9/00756 (MAESTRO 9), and MNiSW grant DIR/WK/2018/12.

DATA AVAILABILITY

The data and softwares used in this research are available at NASA’s HEASARC webpages with the links given in the manuscript.

REFERENCES

- Abdo A. A., et al., 2010, *ApJ*, 716, 30
- Abdollahi S., et al., 2020, *ApJS*, 247, 33
- Acero F., et al., 2015, *ApJS*, 218, 23
- Agarwal A., et al., 2019, *MNRAS*, 488, 4093
- Agrawal P. C., 2017, *Journal of Astrophysics and Astronomy*, 38, 27
- Arnaud K. A., 1996, in Jacoby G. H., Barnes J., eds, *Astronomical Society of the Pacific Conference Series Vol. 101, Astronomical Data Analysis Software and Systems V*. p. 17
- Breeveld A. A., Landsman W., Holland S. T., Roming P., Kuin N. P. M., Page M. J., 2011, in McEnery J. E., Racusin J. L., Gehrels N., eds, *American Institute of Physics Conference Series Vol. 1358, American Institute of Physics Conference Series*. pp 373–376 ([arXiv:1102.4717](https://arxiv.org/abs/1102.4717)), doi:10.1063/1.3621807
- Britzen S., et al., 2018, *MNRAS*, 478, 3199
- Carini M. T., Miller H. R., Noble J. C., Goodrich B. D., 1992, *AJ*, 104, 15
- Dai Y., Wu J., Zhu Z.-H., Zhou X., Ma J., 2011, *AJ*, 141, 65
- Dey L., et al., 2018, *ApJ*, 866, 11
- Dickey J. M., Lockman F. J., 1990, *Annual Review of Astronomy and Astrophysics*, 28, 215
- Gehrels N., et al., 2004, *The Astrophysical Journal*, 611, 1005
- Giommi P., et al., 2006, *A&A*, 456, 911
- Goyal A., 2018, *Galaxies*, 6
- Grupe D., Komossa S., amp Falcone A., 2017, *The Astronomer’s Telegram*, 10043, 1
- Gupta A. C., et al., 2019, *AJ*, 157, 95
- Harrison F. A., et al., 2013, *ApJ*, 770, 103
- Hervet O., Boisson C., Sol H., 2016, *A&A*, 592, A22
- Hosokawa R., Adachi R., Murata K. L., Niwano M., Ogawa F., Nakamura N., Yatsu Y., Kawai N., 2020, *The Astronomer’s Telegram*, 13755, 1
- Ikejiri Y., et al., 2011, *PASJ*, 63, 639
- Jansen F., et al., 2001, *A&A*, 365, L1
- Jermak H., Steele I. A., Lamb G. P., Valtonen M., Zola S., 2016, *Proceedings of the International Astronomical Union*, 12, 241–242
- Kapanadze B., et al., 2018, *The Astrophysical Journal Supplement Series*, 238, 13
- Komossa S., Grupe D., 2020, *The Astronomer’s Telegram*, 13785, 1
- Komossa S., Grupe D., Parker M. L., Valtonen M. J., Gómez J. L., Gopakumar A., Dey L., 2020a, *MNRAS*, 498, L35
- Komossa S., Grupe D., Gomez J. L., 2020b, *The Astronomer’s Telegram*, 13658, 1
- Komossa S., et al., 2021, arXiv e-prints, p. [arXiv:2105.01479](https://arxiv.org/abs/2105.01479)
- Kushwaha P., Sahayanathan S., Singh K. P., 2013, *Monthly Notices of the Royal Astronomical Society*, 433, 2380
- Kushwaha P., et al., 2018a, *MNRAS*, 473, 1145
- Kushwaha P., et al., 2018b, *MNRAS*, 479, 1672
- Kushwaha P., Pal M., Kalita N., Kumari N., Naik S., Gupta A. C., de Gouveia Dal Pino E. M., Gu M., 2020, arXiv e-prints, p. [arXiv:2010.14431](https://arxiv.org/abs/2010.14431)
- Laine S., et al., 2020, *ApJ*, 894, L1
- Lehto H. J., Valtonen M. J., 1996, *ApJ*, 460, 207
- Mao L. S., 2011, *New Astron.*, 16, 503
- Massaro E., Perri M., Giommi P., Nesci R., 2004, *A&A*, 413, 489
- Nilsson K., et al., 2018, *A&A*, 620, A185
- Padovani P., Giommi P., 1995, *ApJ*, 444, 567
- Pian E., et al., 1998, *ApJ*, 492, L17
- Poole T. S., et al., 2008, *MNRAS*, 383, 627
- Prince R., Khatoun R., Stalin C. S., 2021, *Monthly Notices of the Royal Astronomical Society*, 502, 5245
- Raiteri C. M., et al., 2013, *MNRAS*, 436, 1530
- Raiteri C. M., et al., 2015, *Monthly Notices of the Royal Astronomical Society*,

- 454, 353
- Reinhart D., et al., 2020, The Astronomer's Telegram, [13677](#), 1
- Roming P. W. A., et al., 2005, [Space Sci. Rev.](#), **120**, 95
- Schlafly E. F., Finkbeiner D. P., 2011, [ApJ](#), **737**, 103
- Siejkowski H., Wiercholska A., 2017, [Monthly Notices of the Royal Astronomical Society](#), **468**, 426
- Sillanpaa A., Haarala S., Valtonen M. J., Sundelius B., Byrd G. G., 1988, [ApJ](#), **325**, 628
- Singh K. P., et al., 2016, in den Herder J.-W. A., Takahashi T., Bautz M., eds, Society of Photo-Optical Instrumentation Engineers (SPIE) Conference Series Vol. 9905, Space Telescopes and Instrumentation 2016: Ultraviolet to Gamma Ray. p. 99051E, [doi:10.1117/12.2235309](#)
- Singh K. P., et al., 2017, [Journal of Astrophysics and Astronomy](#), **38**, 29
- Valtonen M. J., et al., 2019, [ApJ](#), **882**, 88
- Vaughan S., Edelson R., Warwick R. S., Uttley P., 2003, [MNRAS](#), **345**, 1271
- Wiercholska A., Ostrowski M., Stawarz Ł., Wagner S., Hauser M., 2015, [A&A](#), **573**, A69
- Yadav J. S., et al., 2016, in den Herder J.-W. A., Takahashi T., Bautz M., eds, Society of Photo-Optical Instrumentation Engineers (SPIE) Conference Series Vol. 9905, Space Telescopes and Instrumentation 2016: Ultraviolet to Gamma Ray. p. 99051D, [doi:10.1117/12.2231857](#)
- Zola S., et al., 2020, The Astronomer's Telegram, [13637](#), 1